Data Repository to "Complementary crystal accumulation and rhyolite melt segregation in a late Miocene Andean pluton"

Allen J. Schaen, John M. Cottle, Brad S. Singer, C. Brenhin Keller, Nicolas Garibaldi, and Blair Schoene

LASS U-Pb METHODOLOGY

U-Pb zircon ages and trace element geochemistry were obtained by in situ laser ablation split stream mass spectrometry at the University of California-Santa Barbra following the methods of Kylander-Clark et al. 2013. Zircon with magmatic textures were selected using cathodoluminescence images and ablated with 20 µm spots. The resulting analyte was split into a multi-collector ICP-MS for U-Pb isotopic analysis while simultaneously measuring trace elements using a quadrupole ICP-MS. Whole rock major and trace element geochemistry was generated by XRF and ICP-MS respectively at Washington State University.

We intentionally refrain from calculating weighted means or other statistical treatment to obtain singular U-Pb zircon dates for individual hand samples. Such treatment of requires arbitrary filtering of datasets which span ~600 k.y. in order to produce an accepted MSWD of ~1. This may produce a singular age but it would not be geologically meaningful for a plutonic hand sample. Although we show distinct chemical populations for coeval samples of the Huemul pluton, within the precision of the LA technique we are unable to accurately filter our dates by time on the hand sample scale (see arguments laid out in section 6.1 of Samperton et al., 2015). We note that at least two obvious Risco Bayo antecrysts are present in Huemul Afs granite samples RB1515 and HU1503.

MODELING SETUP AND PARITION COEFFICENTS

Model setup for mafic fractional crystallization curves in Figures 2A, B, and C use the same starting composition and Kds for Rb. Theoretical mafic parent similar to ones used in this region of the Andes (Costa and Singer, 2002).

Starting Composition:

Rb	49	ppm
Ba	300	ppm
Zr	90	ppm
Th	5.5	ppm

mineral	mode	K_D				
		Rb	Zr	Th	Ba	
plag	0.35	0.300	0.010	0.110	1.050	
hbl	0.35	0.290	0.500	0.160	0.387	
cpx	0.15	0.031	0.100	0.030	0.026	
olivine	0.15	0.010	0.012		0.010	
	1.00	0.21	0.20	0.10	0.51	Bulk D

Partition coefficients from Rollinson, 1993; Bacon & Druitt, 1988

Silicic models on Figure 2B, C use the same starting composition. Bracketing fractional crystallization models in Figure 2C are made with end member partition coefficients. Fractionating mineral assemblage resembles that in the Huemul qtz monzonites. Melt evolution determined by the Rayleigh fractionation (Eq.1) and bulk cumulate evolution (Eq.2) equations:

$$\frac{C_L}{C_0} = F^{(D-1)}$$
(Eq.1)

$$\frac{C_R}{C_0} = \frac{1-F^D}{1-F}$$
(Eq. 2)

Where C_L is the trace element concentration in the liquid, C_0 is the initial trace element concentration in the starting magma, C_R is the trace element concentration in the total residual solid, F is the fraction of melt remaining, and D is the bulk partition coefficient. Equations from Albarede, 1995.

Starting Composition:

Rb	182	ppm
Ba	652	ppm

mineral	mode	low K$_D$	
		Rb	Ba
qtz	0.14		
plag	0.35	0.04	0.31
kspar	0.3	0.34	6.12
bio	0.1	2.24	5.37
hbl	0.1	0.01	0.04
magnetite	0.01		
apatite	0.001		
zircon	0.002		
	1.00	0.34	2.49 Bulk D

mineral	mode	high K$_D$	
		Rb	Ba
qtz	0.14		
plag	0.35	0.11	1.52
kspar	0.3	0.74	17.10
bio	0.1	4.20	23.53
hbl	0.1	0.40	0.28
magnetite	0.01		
apatite	0.001		
zircon	0.002		
	1.00	0.72	8.04 Bulk D

Partition coefficients from Rollinson, 1993; Bacon & Druitt, 1988; Mahood & Hildreth, 1983; Bachmann et al., 2005.

Crystallization models in Figure 2B use the same starting composition as Figure 2C but account for zircon saturation (Boehnke et al., 2013). We are unable to model Zr evolution using Kds as in 2C because partitioning will not approximate a Henry's Law relationship due Zr being a stochiometric constituent of zircon. Instead we compare a crystallization model without zircon present (thus Zr is incompatible) to the minimum Zr evolution required to saturated zircon. This is done following the methods of Keller et al. 2017 using the zircon saturation equation of

Boehnke et al. 2013 with calculated temperature and major element (M parameter) evolution generated from alphaMELTS (Smith and Asimow, 2005) using the same starting composition. We take the minimum of these two models as our Zr evolution liquid curve which now accounts for zircon saturation without any assumptions of crystal fraction or partitioning. Once zircon saturates we then assume any Zr not in the melt is in the solids to measure the bulk cumulate evolution. A check of our melt and cumulate curves is performed to ensure mass balance is maintained (Table DR3).

Eu mass balance calculations were performed on the Huemul domains following mixing equation 3:

$$C^{mix} = X^{Afs} * C^{Afs} + (1 - X^{Afs}) * C^{QM}$$ (Eq.3)

Where C^{Afs}, and C^{QM} are average whole rock concentrations of either Sm, Eu, or Gd in the Afs granite and qtz monzonite domains respectively. X^{Afs} is the modelled fraction of Afs granite melt extracted from a mush with starting composition equal to Huemul granite. Mass balances for each element are calculated separately using equation 3 and then used in the calculation of the Eu anomaly (Eu/Eu*). In this way the Eu/Eu* of the granite domain can be compared to the Eu/Eu* obtained via mass balance (Table DR4). Rare earth element plots in Figure 2D are normalized to chondrite of Sun and McDonough, 1989.

GEOLOGIC DOMAINS

Throughout the manuscript, we rely on designation of distinct magmatic domains which have been established through a combination of geologic mapping of lithologies, bulk rock geochemistry, U-Pb zircon age ranges, and zircon trace element geochemistry. These group names, which in detail contain some lithologic variation typical of granitoids (Fig. DR3), are used for convenience and encompass more observations than solely rock type.

References:

Albarede, F., 1995, Introduction to Geochemical Modeling. Cambridge University Press. New York.

Bachmann, O., Dungan, M. A., and Bussy, F., 2005, Insights into shallow magmatic processes in large silicic magma bodies: the trace element record in the Fish Canyon magma body, Colorado: Contributions to Mineralogy and Petrology, v. 149, no. 3, p. 338–349, doi: 10.1007/s00410-005-0653-z.

Bacon, C.R., and Druitt, T.H., 1988, Compositional evolution of the zoned calcalkaline magma chamber of Mount Mazama, Crater Lake, Oregon: Contributions to Mineralogy and Petrology, v. 98, no. 2, p. 224–256, doi: 10.1007/BF00402114.

Boehnke, P., Watson, E.B., Trail, D., Harrison, T.M., and Schmitt, A.K., 2013, Zircon saturation re-revisited: Chemical Geology, v. 351, p. 324–334, doi: 10.1016/j.chemgeo.2013.05.028.

Costa, F. & Singer, B., Evolution of Holocene dacite and compositionally zoned magma, Volcán San Pedro, southern volcanic zone, Chile. J. Petrol. 43, 1571–1593 (2002).

Keller, C.B., Boehnke P., Schoene, B., 2017, Temporal variation in relative zircon abundance throughout Earth history: Geochemical Perspectives Letters v. 3, p. 179-189, doi: 10.7185/geochemlet.1721.

Kylander-Clark, A.R.C., Hacker, B.R., and Cottle, J.M., 2013, Laser-ablation split-stream ICP petrochronology: Chemical Geology, v. 345, p. 99–112, doi: 10.1016/j.chemgeo.2013.02.019.

Mahood, G.A., and Hildreth, W., 1983, Large partition coefficients for trace elements in high-silica rhyolites: Geochimica et Cosmochimica Acta, v. 47, p. 11–30.

Rollinson, H.R., 1993, Using geochemical data: evaluation, presentation and interpretation. Pearson Education Limited, Harlow.

Samperton, K., Schoene, B., Cottle, J.M., Keller, C.B., Crowley, J.L., Schmitz, M., 2015, Magma emplacement, differentiation and cooling in the middle crust: Integrated zircon geochronological–geochemical constraints from the Bergell Intrusion, Central Alps: Chemical Geology, v. 417, p. 322-340, doi:10.1016/j.chemgeo.2015.10.024.

Smith, P.M., and Asimow, P.D., 2005, Adiabat-1ph: A new public front-end to the MELTS, pMELTS, and pHMELTS models: Geochemistry, Geophysics, Geosystems, v. 6, no. 2, p. 1–8, doi: 10.1029/2004GC000816

Streckeisen, A., 1979, Classification and nomenclature of volcanic rocks, lamprophyres, carbonatites, and melilitic rocks: Recommendations and suggestions of the IUGS Subcommission on the Systematics of Igneous Rocks: Geology, v. 7, p. 331–335, doi: 10.1130/0091-7613(1979)7<331.

Sun, S. -s., and McDonough, W.F., 1989, Chemical and isotopic systematics of oceanic basalts: implications for mantle composition and processes: Geological Society, London, Special Publications, v. 42, no. 1, p. 313–345, doi: 10.1144/GSL.SP.1989.042.01.19.

Vance, J.A., 1969, On synneusis: Contributions to Mineralogy and Petrology, v. 24, no. 1, p. 7–29, doi: 10.1007/BF00398750.

Tables DR1-DR4

Figure Captions:

**Figure DR1:** Photos of field relationships, magmatic contacts, and miarolitic cavities in the RBH pluton.

Figure DR2: Map of RBH pluton with added cross section lines A-A' (no vertical exaggeration) and B-B''' (vertical exaggeration of ~2). Solid lines are sharp contacts; dashed lines are gradational contacts; dotted lines are inferred.

Figure DR3: QAP ternary of rocks from the Risco Bayo-Huemul pluton. Normalized to 100 modal % of quartz (Q), alkali feldspar (A), and plagioclase (P). Fields represent [1] alkali feldspar granite; [2] syenogranite; [3] monzogranite; [4] granodiorite; [5] tonalite; [6] quartz alkali feldspar syenite; [7] quartz syenite; [8] quartz monzonite; [9] quartz monzodiorite, quartz monzograbbro; [10] quartz diorite, quartz gabbro, quartz anorthosite; [11] diorite, gabbro. Fields from Streckeisen, 1976.

Figure DR4: Harker diagrams of Risco Bayo-Huemul plutonic complex. A notable compositional gap is present within the Huemul pluton between ~70 and 75 wt.% SiO_2 in most elements.

Figure DR5: Full thin section xpl/ppl images (~27 x 46 mm, n=4) and enlarged xpl photomicrographs (n=7) of porphyritic qtz monzonites from the Huemul pluton. The textural features we suggest might be cumulative include: concentration of mostly interlocking euhedral feldspars with intestinal finer-grained aggregates of anhedral quartz and kspar; different zoning patterns of adjacent feldspars; coarse grained concentrations of plagioclase; and synneusis textures (Vance, 1969).

Figure DR6: Example cathodoluminescence images of RBH zircon analyzed by LASS.

Figure DR1

Roof exposure of the Huemul pluton in contact with hornfels wallrock (MV) and Tatara-San Pedro lavas (TSP).
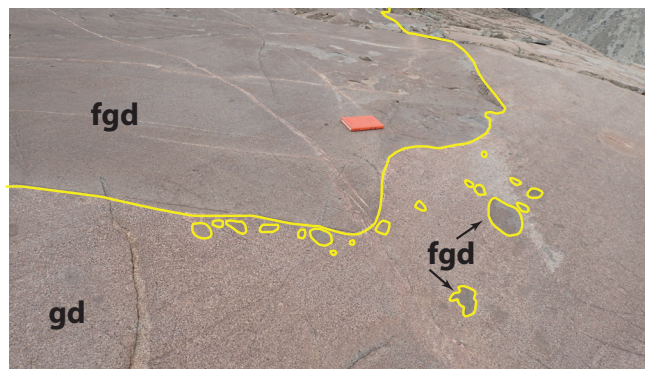
Example Risco Bayo magmatic contact between the fine grained diorite (fgd) and granodiorite (gd) domains.

Example Risco Bayo magmatic contact between the fine grained diorite (fgd) and gabbro (g) domains.
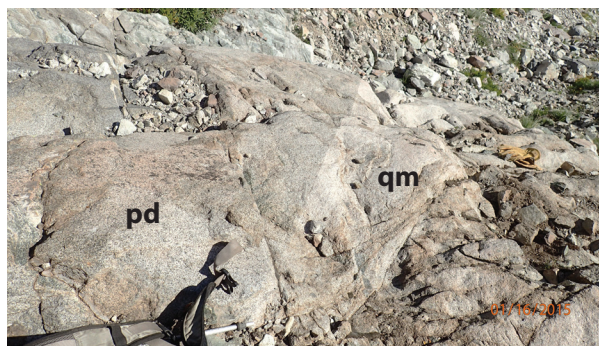

Magmatic contact between Risco Bayo porphyritic diorite (pd) and Huemul qtz monzonites (qm).

Portion of the ~2000 m^2 zone of miarolitic cavities in Huemul Afs granite domain showing. Cavitiy abundance estimated at ~10 vol.%
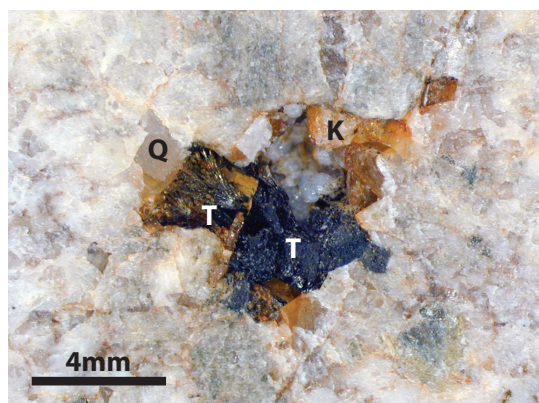
Hand sample of Huemul Afs granite from the miarolitic cavity outcrop (left). Enlargement of individual cavity (right) infilled with euhedral tourmaline (T), kspar (K). and quartz.

Figure DR2
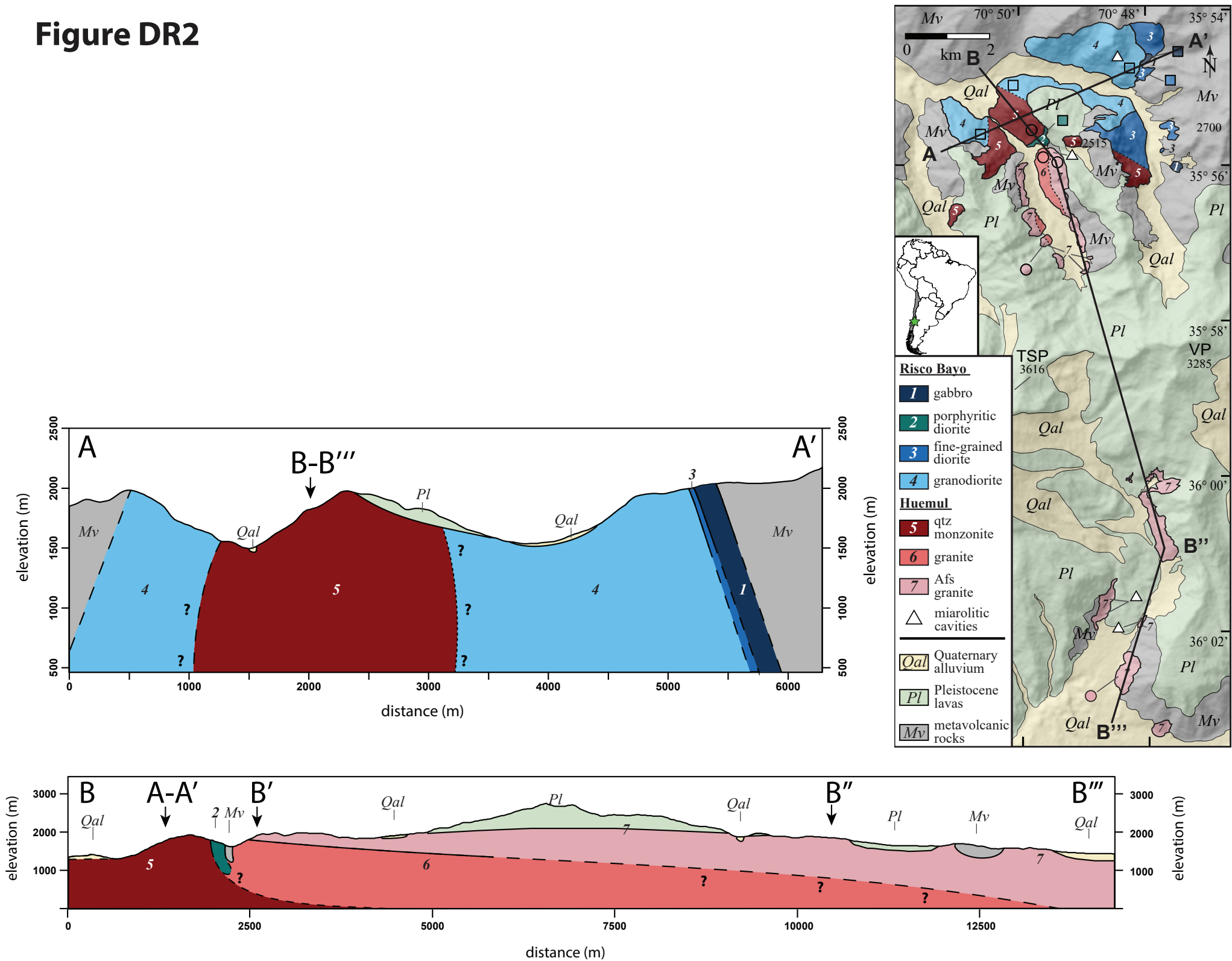
Figure DR3
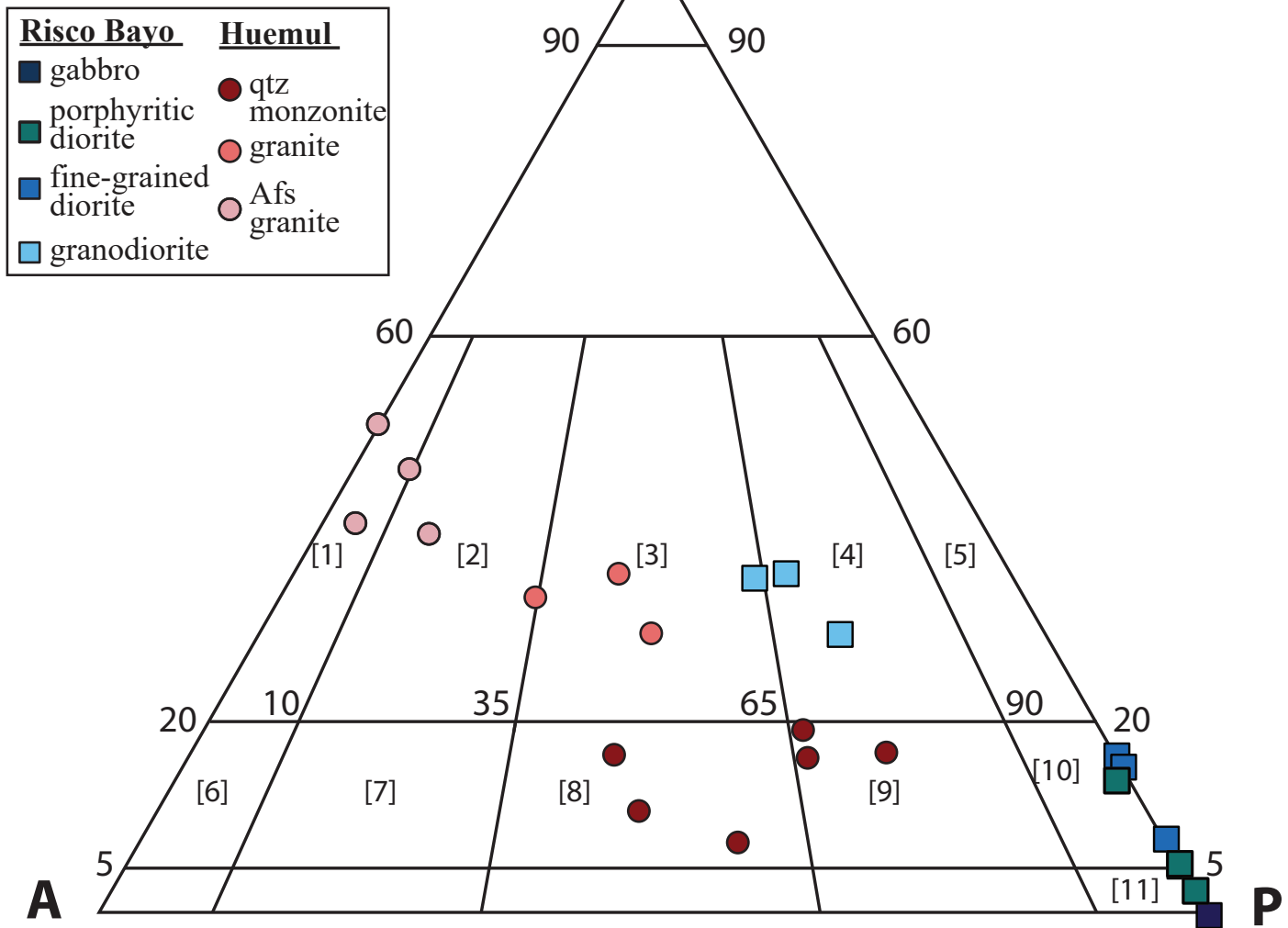
Figure DR4
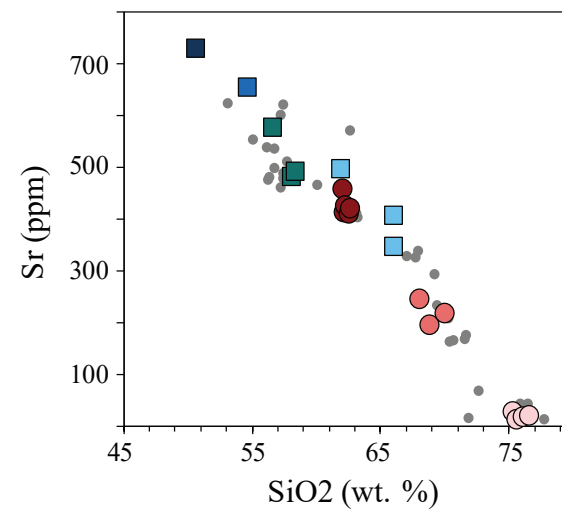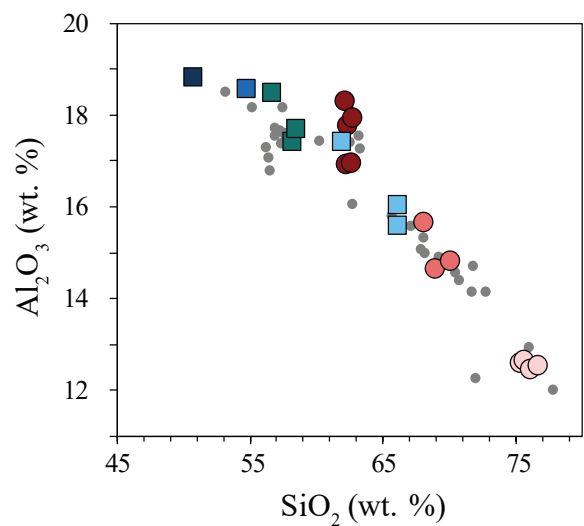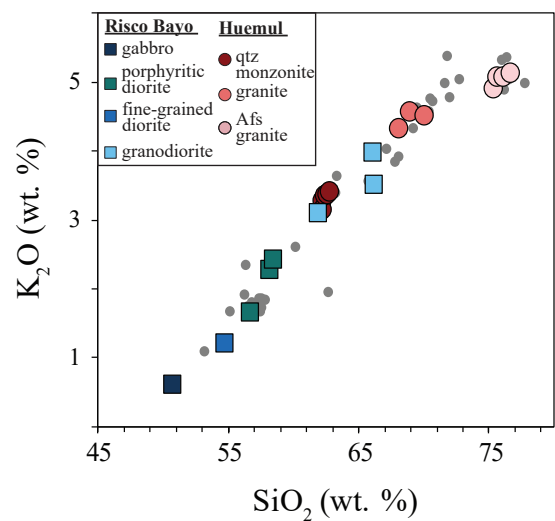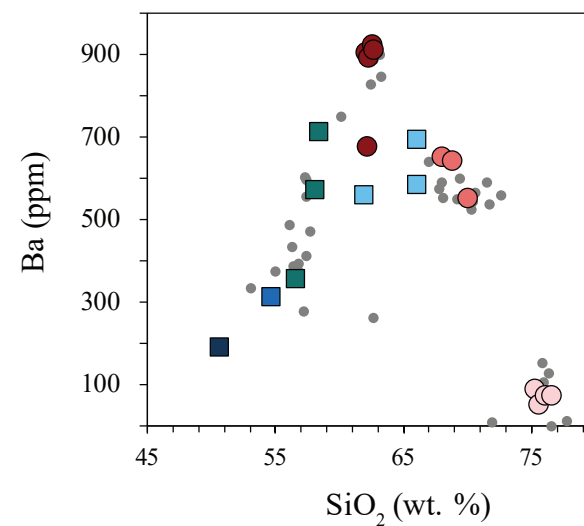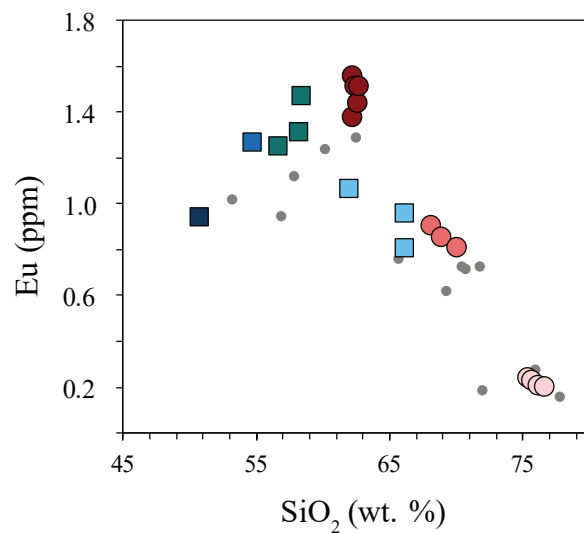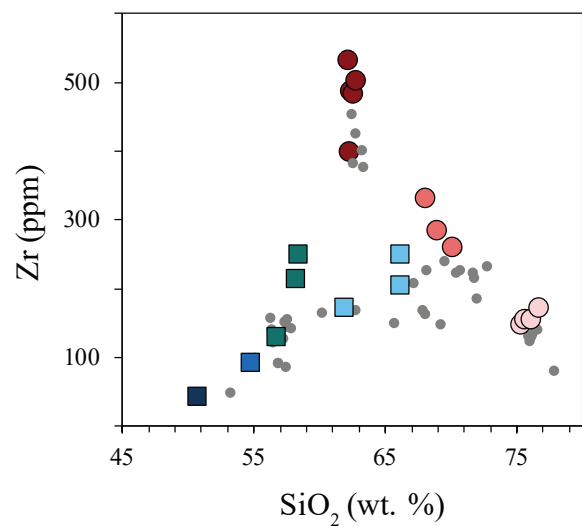
Figure DR5

RB1507
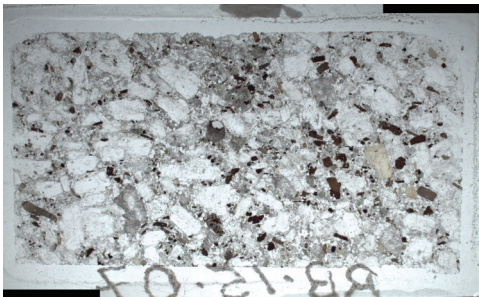
RB1511
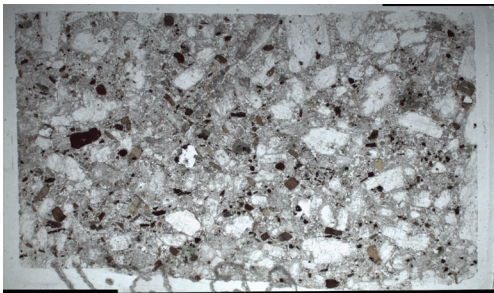
RB1511
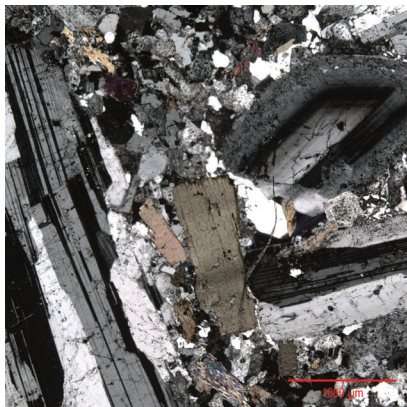
RB1510
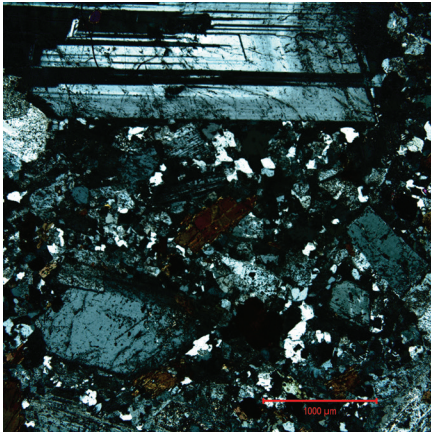
RB1501
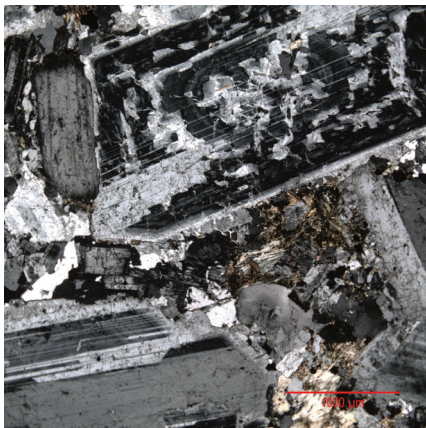
RB1501
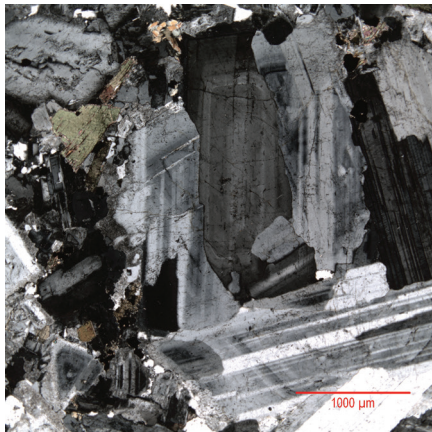
HC1305
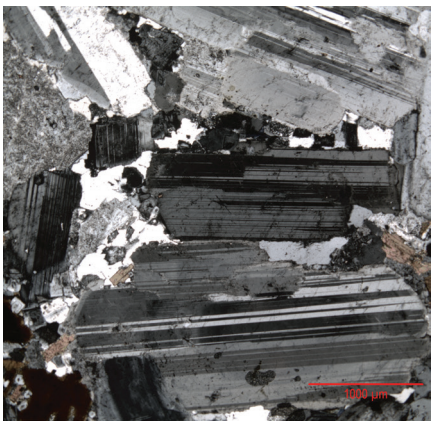
RB1507

RB1507

Figure DR6